Investigation of nickel electrochemical impedance spectra under conditions of anodic polarization in hydroxide solutions with chloride ion additives

V.E. Kasatkin,* L.P. Kornienko, A.I. Shcherbakov, I.V. Kasatkina, I.G. Korosteleva and V.N. Dorofeeva

A.N. Frumkin Institute of Physical Chemistry and Electrochemistry, Russian Academy of Sciences, Leninsky pr. 31, 119071 Moscow, Russian Federation
**E-mail: danab13@yandex.ru*

Abstract

Nickel in a slightly alkaline medium with chloride additives was chosen as a model system for studying a metal prone to passivation and the formation of point defects during anodic polarization. For this system, electrochemical impedance spectra were obtained at different ratios of concentrations of sodium hydroxide and chloride under conditions of anodic polarization. We intended to use them to assess the thickness and uniformity of the passive layer on the metal surface. The existence of two time constants, manifested in the high frequency and low-frequency regions, was found on the impedance spectra. To process the EIS results, Mansfeld's equivalent circuit was chosen which corresponds to the physical model of a metal with an oxide layer on the surface. It is shown that at high frequencies, the charge transfer at the interface between the solution and the oxide layer is performed by anions. The low-frequency part of the impedance spectrum is due to the Faraday process of solid-phase oxidation of nickel at the oxide and metal interface. As in the previously studied chloride free system, the same patterns are observed: a power-law dependence of the resistance to ion charge transfer across the oxide layer/solution boundary on the concentration of anions has been established, which can be described in terms of the Freundlich isotherm. Moreover, this charge transfer resistance is practically independent of the potential. The capacitance of the double layer at the same boundary is directly proportional to the square root of the total concentration of alkali and chloride, which indicates compliance with the classical Gui–Chapman model. With an increase in the anodic potential and the concentration of anions, there is a tendency to decrease the resistance and increase the capacitance factor of the Faraday reaction. According to the resistance values related to the high-frequency part of the impedance spectrum and the overall capacitance of the double electric layer, it is not possible to track the change in the thickness of the oxide layer formed on the surface during anodic polarization.

Received: March 19, 2024. Published: April 1, 2024 doi: 10.17675/2305-6894-2024-13-2-3

Keywords: *nickel, alkaline medium, chloride, electrochemical impedance spectroscopy.*

Introduction

Nickel is used in industry as a structural material for the manufacture of chemical [1, 2] and special equipment [3], as a catalyst for many chemical processes [4–7, 29], as a material for anticorrosive coatings [8–11] and as an electrode material in the manufacture of batteries [12, 13, 34]. Its electrochemical behavior has been well studied [7, 14–18, 31, 32]. It, like stainless steels, is prone to passivation due to the formation of oxidation products films on the surface that are resistant to a corrosive environment and prevents further corrosion destruction of the metal. The composition, structure and thickness of the surface films on the metal determine the degree of passivation and conditions in which there are violations of their continuity caused by the appearance of pitting corrosion. One of the strongest factors causing pitting is the presence of chloride ions in the solution [19–21, 33].

Pure metallic nickel, unlike multicomponent stainless steels (which can also include it in their composition), is a convenient object for modeling. It is a single-component metal, the properties of which have been well studied [7, 29]. Therefore, this metal was chosen as a model object for studying the effect of the thickness of the oxide–hydroxide passive film formed on the nickel surface during anodic polarization in an alkaline medium on the patterns of pitting formation in the presence of chlorides in solution.

To control the thickness of the passive films formed, it was assumed to use the method of electrochemical impedance spectroscopy (EIS). This method has found wide application in modern research, since it allows obtaining information about the state of the surface of the metal under study in a corrosive environment, including under the influence of external polarization [11].After processing the EIS results in terms of an equivalent circuit, it was assumed that the values of the nominal values of the capacitive and resistive circuit elements would estimate the change in thickness (and integrity) of surface oxide–hydroxide films on metal, depending on the conditions of their formation [22]. In other words, we assumed that the capacitance of the element which is related to a high-frequency process in the equivalent circuit should be inversely proportional to the thickness of the formed resistive surface film, and the resistance of this element increases with increasing thickness.

Although high-frequency arcs, which were observed in the Nyquist diagrams traditionally, associated with the appearance of poorly conductive layers on the metal surface, it turned out that their shape practically does not depend on the potential and duration of polarization in solutions of the same composition [23]. These experimental results contradicted our expectations, since an increase in the polarization potential and time cannot but affect the thickness of the surface film and its continuity [24]. Obviously, the thickness of the oxide–hydroxide film on nickel should increase over time with anodic polarization in an alkaline medium. In addition, pitting corrosion occurs in chloride-containing solutions at high anodic potentials, which violates the uniformity of the surface film [25]. At the same time, no significant changes in the shape of high-frequency arcs are noticeable on the impedance spectra obtained in solutions of the same composition, even at

high anode potentials, when the low-frequency hodograph arcs take the form of a pseudo-inductive loop [11, 23]. The latter indicates the appearance of local pitting corrosion lesions.

Thus, the nature of the high-frequency section of the electrochemical impedance spectrum of nickel samples turned out to be insensitive to changes in the thickness of the oxide–hydroxide film formed on the surface during their polarization in an alkaline medium. At the same time, the change in concentration had a significant effect on the elements of the impedance spectrum. For experiments in NaOH solutions, the dependence of the resistance and capacitance of high-frequency elements of the equivalent circuit on the alkali concentration of has been established [26]. This publication continues the study of the nature of the electrochemical impedance spectra on nickel in slightly alkaline NaOH media with different chloride contents.

Experimental Technique

Chemical grade reagents were used to prepare NaOH solutions with NaCl additives. As in our previous studies [23, 26], the experiments were carried out at 30°C in a three-electrode cell with natural aeration of the solution. A high purity nickel cylinder with 3.62 cm^2 working surface served as a working electrode. Before each individual measurement, it was ground on M40 abrasive paper and fixed coaxially in a current supply isolated from the electrolyte. We used a saturated silver chloride reference electrode. All potentials are given relative to this electrode. The auxiliary electrode was made of platinum. Special measures were taken to prevent the penetration of Cl^- ions from the electrolytic bridge and to accurately fix its position relative to the sample surface.

EIS measurements were carried out using an IPC-Pro MF potentiostat with an impedance unit FRA-2 (Russia) in the frequency range from 5 kHz to 0.15 Hz with harmonic signal amplitude of 10 mV. The experiments were carried out in a potentiostatic mode, starting with the "open circuit" potential, and then the potential was shifted anodically in increments of 100 mV to achieve potentials causing a sharp increase in the anode current, which indicates a violation of the passive state of nickel. At each potential value, the impedance spectrum was taken.

Based on the obtained EIS data, the optimal equivalent circuit was selected. Using specially developed software Dummy Circuits Solver, the values of the equivalent circuit elements were calculated. Nyquist and Bode diagrams were built using ZMonitor software.[1]

Results and Discussion

Nyquist diagrams for nickel in an alkaline medium in the presence of chlorides have a characteristic shape in the form of two semicircles. The same form of the diagrams was obtained earlier [23] in electrolytes without chloride additives. We studied NaOH solutions at the concentrations of 0.001 M, 0.01 M and 0.1 M with and without chloride ions addition

[1]The Dummy Circuits Solver and ZMonitor programs were developed by V.E. Kasatkin specifically for working with the IPC-FRA electrochemical complex.

(0.0005 M, 0.001 M and 0.003 M). For example, Figure 1 shows sample impedance spectra at different ratios of alkali and chloride concentrations obtained at the same potential E=+170 mV corresponding to the passive state of nickel.

High-frequency arcs of small radius are clearly distinguishable in a solution with the lowest alkali concentration 0.001 M NaOH (Figure 1.1). With an increasing in the sodium hydroxide content by an order of magnitude (0.01 M NaOH), the ratio of radii of low- and high-frequency semicircles on the impedance hodograph changes (Figure 1.2). When the alkali concentration increases by another order of magnitude to 0.1 M NaOH, these high-frequency arcs practically disappear due to the small scale of the initial section (Figure 1.3).

The logarithmic scale of the axes in small diagrams for the high-frequency sections of the spectra (Figure 1.1–1.3) makes it possible to better represent the results. Of course, when using a logarithmic scale, the hodograph arc will not have the shape of regular semicircles typical for parallel connection of RC circuit elements. However, these graphs allow us to demonstrate the similarity of the shape of high-frequency sections of hodographs when the concentration of ions in solution changes by several orders of magnitude, which strongly affects the conductivity of solutions. It is obvious that in a solution with the same concentration of alkali, high-frequency arcs have approximately the same radius, regardless of the concentration of chloride. At the same time, the displacement of the hodographs along the Z_{Re} axis towards lower resistances is clearly noticeable, since the total concentration of ions in the solution increases with the addition of chloride, causing an increase in the conductivity of the electrolyte. This effect is most pronounced at the lowest concentration of alkali, since this solution has the lowest conductivity and even a small addition of chloride significantly increases it (Figure 1.1). Obviously, with an increase in the alkali concentration (and with an increase in the conductivity of the solution), the effect of chloride additives on the overall conductivity will be less and less significant (Figures 1–2 and 1.3). The similarity of the nature of the high-frequency regions in the EIS spectra in experiments with different chloride contents at constant NaOH concentrations is also clearly seen in the Bode phase diagrams (Figure 1.1–1.3).

It should be noted that arcs in the high-frequency part of the impedance spectrum are most noticeable in solutions with a low alkali concentration. With the growth of its content, they are greatly smoothed out. Probably due to the high concentration of alkali (1 M NaOH), the authors [11] did not observe high-frequency arcs on Nyquist diagrams.

The change in the potential (and duration of polarization from the beginning of EIS experiment) has little effect on the shape and radius of the high-frequency arc in the solution of unchanged composition, unlike the shape and the radii of low-frequency semicircles. With an increase in the anodic potential and with an increase in the electrolyte concentration, the radii of the low-frequency arcs of the impedance spectra decrease, and at the highest potentials they take the form of a pseudo-inductive loop. The decrease in the radii of low-frequency arcs is due to the intensification of the Faraday Nickel oxidation process with an increase in anodic polarization. The appearance of a pseudo-inductive loop indicates a violation of the uniformity of the passive film on nickel and the formation of pitting lesions [26, 27].

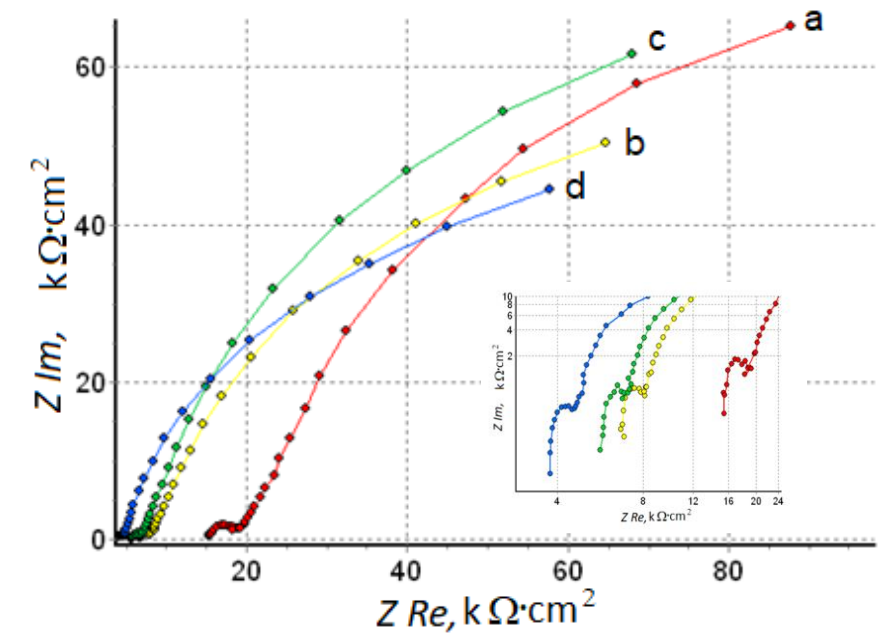

A

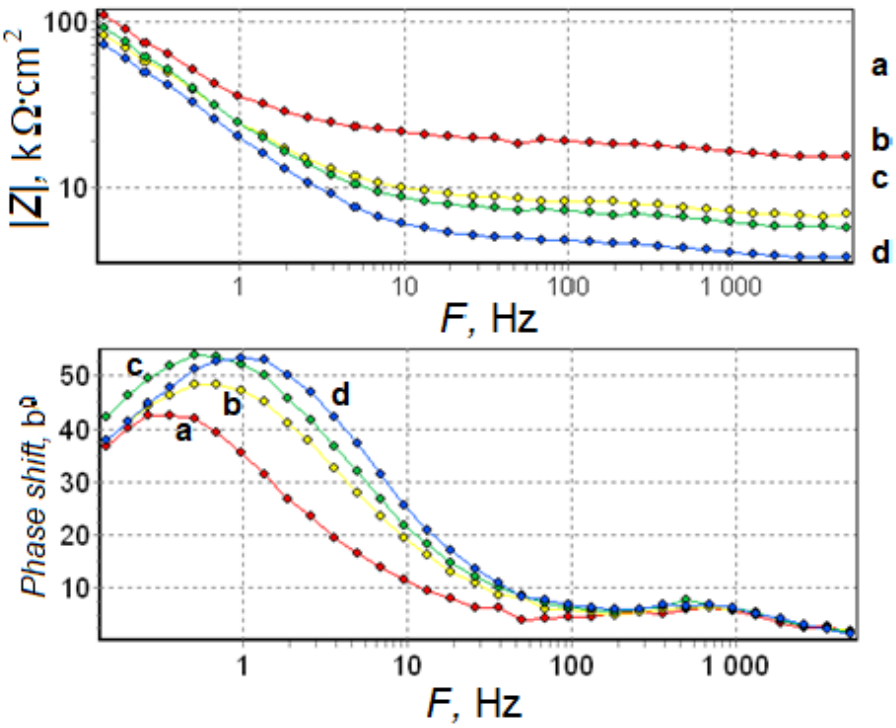

B

Figure 1.1. Nyquist plot (A) and Bode diagram (B) for Nickel at the polarization E=+170 mV in 0.001 M NaOH solutions with chloride additives: a – 0 M, b – 0.0005 M, c – 0.001 M, d – 0.003 M.

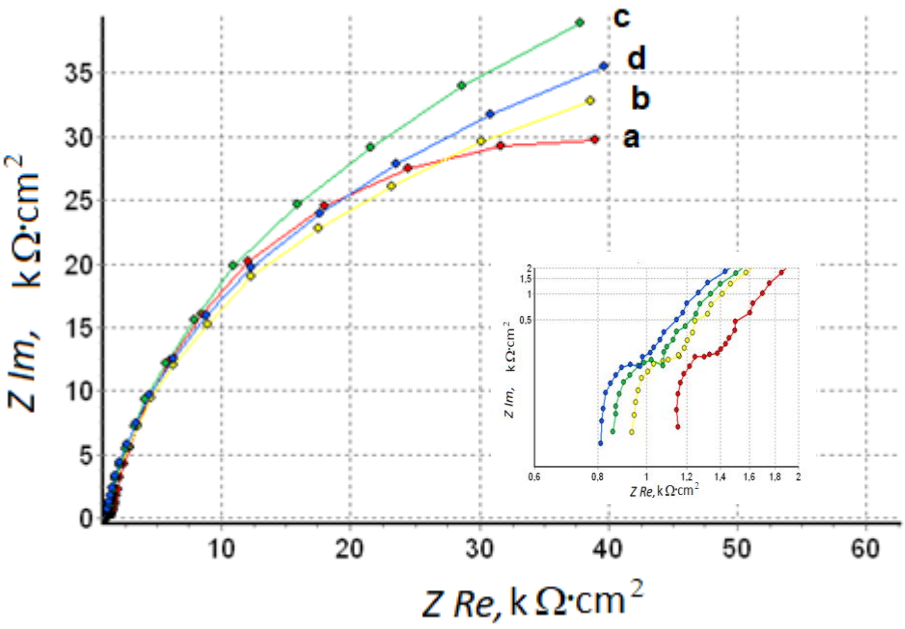

A

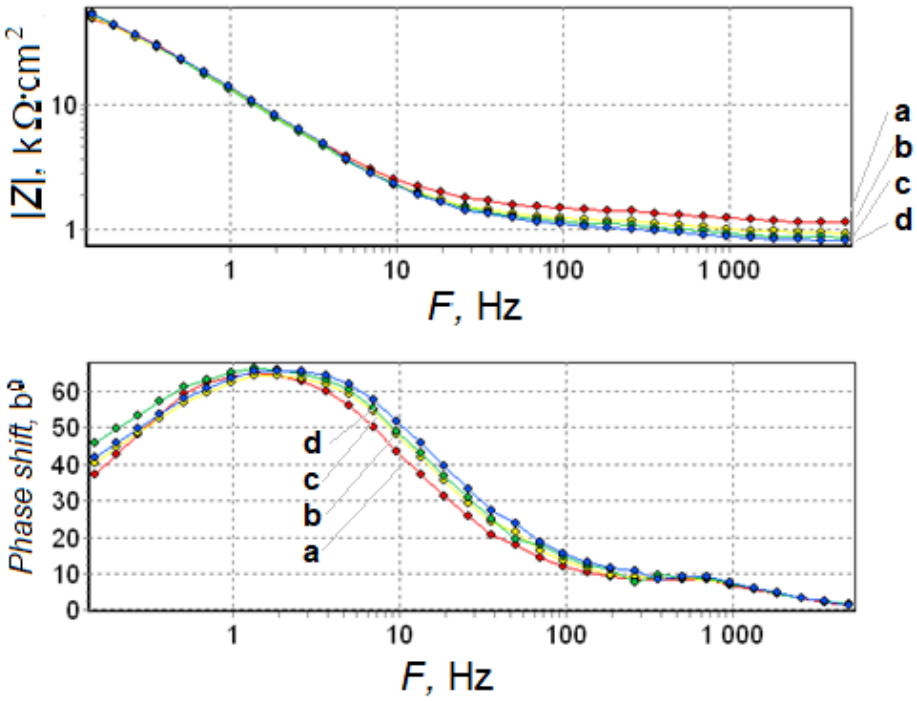

B

Figure 1.2. Nyquist plot (A) and Bode diagram (B) for Nickel at the polarization E=+170 mV in 0.01 M NaOH solutions with chloride additives: a – 0 M, b – 0.0005 M, c – 0.001 M, d – 0.003 M.

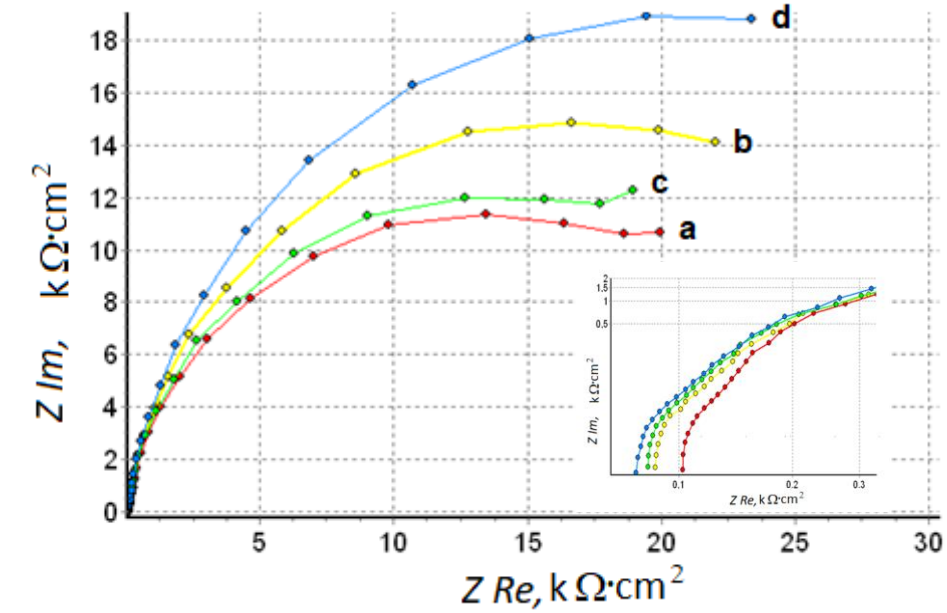

A

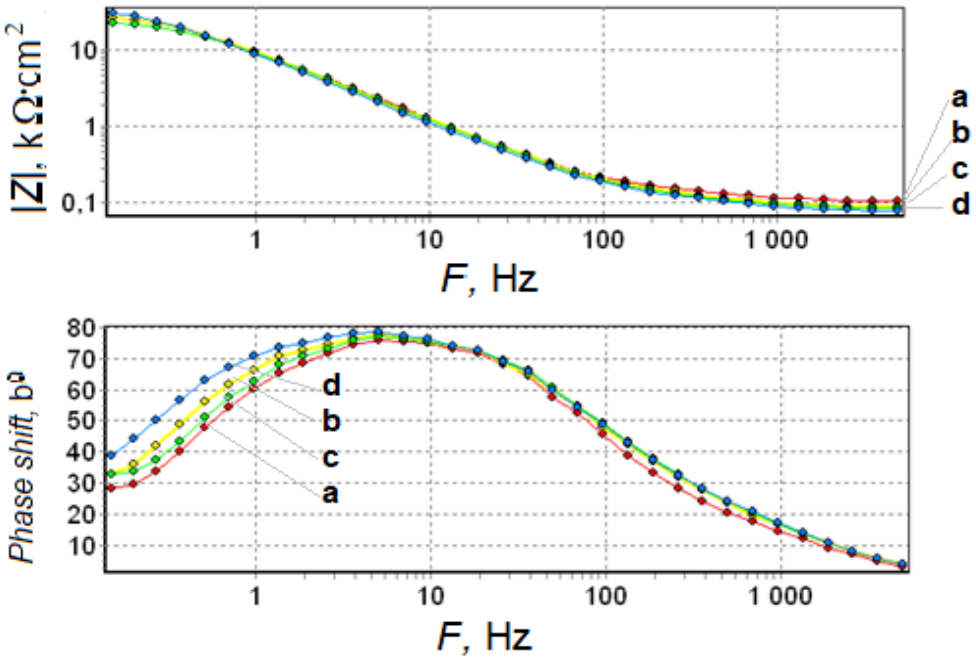

B

Figure 1.3. Nyquist plot (A) and Bode diagram (B) for Nickel at the polarization E=+170 mV in 0.1 M NaOH solutions with chloride additives: a – 0 M, b – 0.0005 M, c – 0.001 M, d – 0.003 M.

These patterns are clearly visible from Figures 2.1–2.3, selected as an illustration for three systems in which NaOH content varies by two orders of magnitude (from 0.01 M to 0.1 M) at the same concentration of Cl^- ions (0.001 M).

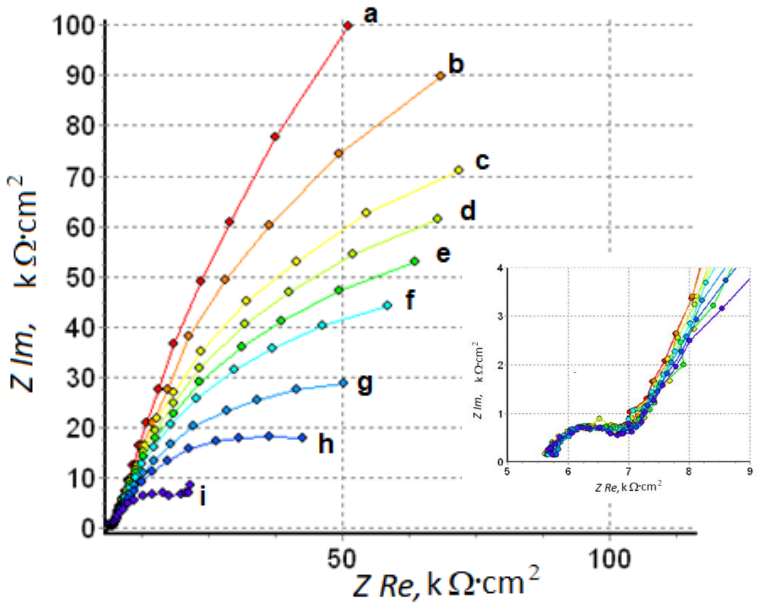

Figure 2.1. Nyquist plot for nickel in the solution of 0.001 M NaOH+0.001 M Cl^- at the polarization: a – E=–270 mV, b – E=–170 mV, c – E=–70 mV, d – E=+70 mV, e – E=+170 mV, f – E=+270 mV, g – E=–370 mV, h – E=–470 mV, i – E=–570 mV.

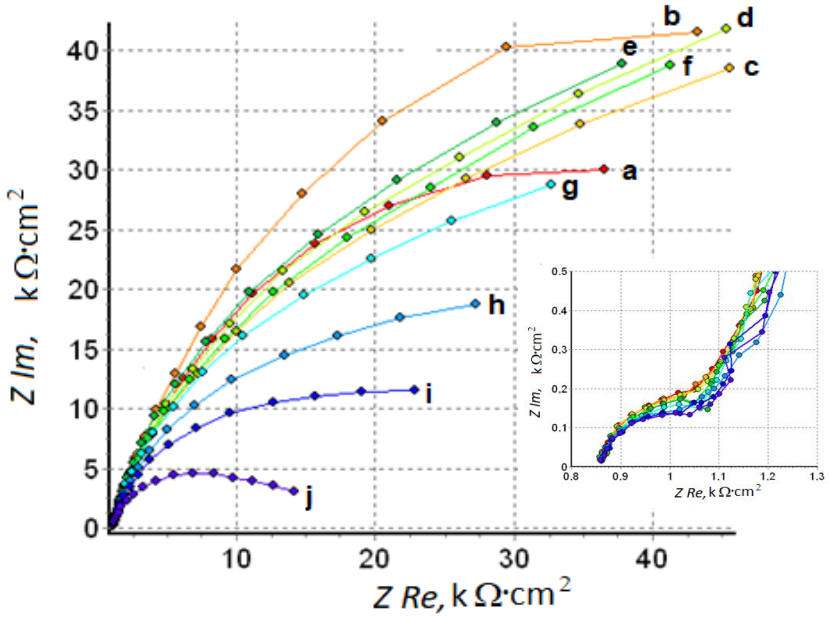

Figure 2.2. Nyquist plot for nickel in the solution of 0.01 M NaOH+0.001 M Cl^- at the polarization: a – E=–380 mV, b – E=–280 mV, c – E=–180 mV, d – E=–80 mV, e – E=+70 mV, f – E=+170 mV, g – E=+270 mV, h – E=–370 mV, i – E=–470 mV, j – E=–570 mV.

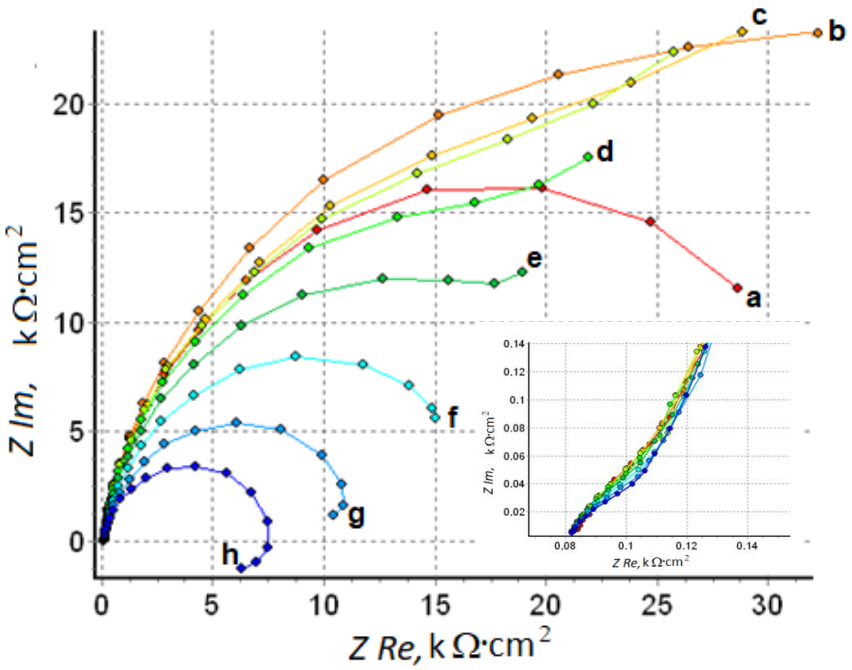

Figure 2.3. Nyquist plot for nickel in the solution of 0.1M NaOH + 0.001M Cl^- at the polarization: a – *E*=–360 mV, b – *E*=–260 mV, c – *E*=–160 mV, d – *E*=–60 mV, e – *E*=+70 mV, f – *E*=+170 mV, g – *E*=+270 mV, h – *E*=–370 mV, i – *E*=–470 mV.

To establish quantitative patterns, the impedance spectra are processed in terms of electing an equivalent circuit adequate to experimental results. All the hodographs obtained in our EIS experiments are formed by a pair of semicircles (*i.e.* they have two time constants). Therefore, an equivalent circuit must contain two pairs of RC elements connected in parallel. The equivalent circuit proposed by F. Mansfeld [27] is well suited for processing impedance spectra on metals with a passive film on the surface (Figure 3).

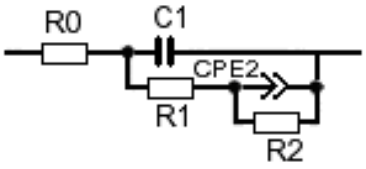

Figure 3. The equivalent circuit for modeling the EIS results.

In this circuit, the resistor R0 corresponds to the resistance of the electrolyte between the tip of the Luggin capillary and the outer surface of the sample. Element C1 corresponds to the capacitance of the double layer formed at the outer boundary of the oxide–hydroxide coating on the metal surface. Resistance R1 simulates the process of charge transfer by ions through the passive oxide–hydroxide layer. The parallel-connected resistor R2 and the constant phase element CPE2 characterize, respectively, the resistance and capacitance of the Faraday process on the surface of metallic nickel. It is obvious that an increase in anode

polarization is accompanied by an increase in the nickel oxidation process, causing an increase in current and, accordingly, a decrease in resistance R2. We used a constant phase element CPE2 instead of the traditional capacitance to better account for the flattening of the low-frequency arc shape. It modulus Q_0 allows you to evaluate the capacitive properties of an element if the phase factor n is close to 1. At the same time, the value of n depends on the diffusion properties of the interface and the uniformity of the sample surface [27].

$$Z_{\mathrm{CPE}} = Q_0^{-1}(j\omega)^{-n}, \quad (1)$$

where ω is the cyclic frequency.

Such equivalent circuit is traditionally used to describe a system where experimental hodographs are formed by two semicircles. However, pseudo-inductive loops arise in the impedance spectra at the highest potentials, requiring the inclusion of additional elements in the circuit [11, 26 and 27]. In order not to complicate the analysis of the results, in this work we limited ourselves to modeling only the potential and frequency regions where the purely capacitive behavior of the electrode takes place. Since pseudo-inductive effects at high potentials are manifested in the region of the lowest frequencies when processing spectra, we have limited the lower frequency boundary when processing spectra so that the fitting error does not exceed 2% (*i.e.* excluding the pseudo-inductive loop zone). The low frequency boundaries used for calculations, as well as the fitting values of the equivalent circuit elements are presented in Tables 1–3.[2]

Table 1. Calculated values of the equivalent circuit elements for 0.001 M NaOH solutions.

***E*, mV**	***I*, μA/cm²**	**R0, kΩ·cm²**	**R1, kΩ·cm²**	**R2, kΩ·cm²**	**C1, μF/cm²**	**CPE2 Q_0, μF·cm^{-2}·s^{n-1}**	**CPE2 *n***	**Low frequency limit, Hz**
0.001 M NaOH								
–370	–0.30	13.579	3.494	124.27	0.0735	9.42	0.756	0.15
–270	0.38	14.149	3.289	173.11	0.0817	9.15	0.766	0.15
–170	1.00	13.680	3.183	161.17	0.0826	8.42	0.774	0.15
–70	1.24	14.563	3.498	140.14	0.0900	8.48	0.783	0.15
30	1.16	14.659	3.514	148.36	0.0816	8.73	0.776	0.15
70	0.65	15.314	3.293	200.35	0.0702	8.96	0.782	0.15
170	1.04	15.505	3.296	144.30	0.0750	10.04	0.758	0.15
270	1.23	15.459	3.912	106.74	0.0796	10.81	0.768	0.15
370	1.20	15.783	3.419	79.83	0.0668	12.38	0.746	0.15
470	1.57	15.776	3.605	31.57	0.0716	13.56	0.780	0.15

[2] The results for the impedance spectra clipped at the lower frequency limit are shown in the tables in italics.

***E*, mV**	***I*, μA/cm²**	**R0, kΩ·cm²**	**R1, kΩ·cm²**	**R2, kΩ·cm²**	**C1, μF/cm²**	**CPE2 Q_0, μF·cm^{-2}·s^{n-1}**	**CPE2 *n***	**Low frequency limit, Hz**
0.001 M NaOH + 0.0005 M Cl⁻								
–450	0.01	6.525	1.580	598.93	0.1765	11.31	0.762	0.15
–350	0.03	6.671	1.986	379.50	0.2234	9.28	0.838	0.15
–250	0.32	6.804	1.826	275.64	0.2492	8.74	0.854	0.15
–150	0.65	6.670	1.860	182.94	0.1990	8.93	0.846	0.15
–50	0.92	6.702	1.793	142.76	0.2008	9.26	0.833	0.15
70	1.27	6.734	1.724	131.35	0.1901	9.89	0.819	0.15
170	0.90	6.703	1.700	130.38	0.1792	10.60	0.810	0.15
270	1.17	6.702	1.659	112.68	0.1682	11.76	0.795	0.15
370	1.34	6.771	1.539	82.95	0.1726	13.46	0.777	0.15
470	1.44	6.777	1.559	59.37	0.1744	15.06	0.775	0.15
570	2.09	6.753	1.573	36.56	0.1827	15.89	0.790	0.15
0.001 M NaOH + 0.001 M Cl⁻								
–270	–0.09	5.758	1.529	626.32	0.2518	9.19	0.841	0.15
–170	0.32	5.803	1.694	276.88	0.2479	8.36	0.864	0.15
–70	0.54	5.717	1.710	187.45	0.2444	8.45	0.853	0.15
40	1.15	5.704	1.627	126.17	0.2172	9.23	0.831	0.15
70	0.71	5.748	1.626	157.46	0.2068	9.19	0.848	0.15
170	0.99	5.796	1.664	136.34	0.2365	9.96	0.833	0.15
270	0.94	5.737	1.533	111.32	0.2375	10.86	0.831	0.15
370	1.30	5.786	1.442	73.43	0.2338	12.41	0.820	0.15
470	1.73	5.718	1.481	49.48	0.2370	13.81	0.821	0.15
570	6.74	5.641	1.245	21.97	0.1911	18.54	0.757	0.15
0.001 M NaOH + 0.003 M Cl⁻								
–320	–0.48	3.709	0.914	92.34	0.2823	11.60	0.815	0.15
–220	0.20	3.774	1.126	130.78	0.3702	10.88	0.868	0.15
–120	1.54	3.784	1.077	87.11	0.2987	10.24	0.840	0.15
–20	1.46	3.787	1.098	103.16	0.3102	9.97	0.855	0.15
70	1.51	3.786	1.083	104.21	0.2998	10.49	0.849	0.15

***E*, mV**	***I*, μA/cm²**	**R0, kΩ·cm²**	**R1, kΩ·cm²**	**R2, kΩ·cm²**	**C1, μF/cm²**	**CPE2 Q_0, μF·cm^{-2}·s^{n-1}**	**CPE2 *n***	**Low frequency limit, Hz**
170	1.39	3.799	1.037	101.20	0.2980	11.37	0.840	0.15
270	1.50	3.798	1.040	88.45	0.2943	12.63	0.834	0.15
370	1.80	3.817	1.005	58.55	0.2985	14.88	0.817	0.15
470	8.65	3.801	0.945	15.97	0.2973	17.01	0.827	0.36

Table 2. Calculated values of the equivalent circuit elements for 0.01 M NaOH solutions.

***E*, mV**	***I*, μA/cm²**	**R0, kΩ·cm²**	**R1, kΩ·cm²**	**R2, kΩ·cm²**	**C1, μF/cm²**	**CPE2 Q_0, μF·cm^{-2}·s^{n-1}**	**CPE2 *n***	**Low frequency limit, Hz**
0.01 M NaOH								
–300	–0.16	1.091	0.497	143.71	1.3095	11.45	0.903	0.15
–280	0.14	1.103	0.458	157.56	1.1121	12.15	0.891	0.15
–180	–0.27	1.117	0.489	171.30	1.1197	11.03	0.903	0.15
–80	0.11	1.129	0.465	107.14	1.0990	11.18	0.898	0.15
40	0.62	1.131	0.430	98.83	0.9870	12.15	0.887	0.15
70	0.00	1.146	0.457	102.72	1.0119	11.74	0.899	0.15
170	0.39	1.151	0.436	68.98	0.9814	12.78	0.895	0.15
270	0.82	1.151	0.436	68.98	0.9814	12.78	0.895	0.15
370	1.82	1.158	0.420	23.18	1.0187	14.92	0.929	0.15
470	1.67	1.168	0.410	16.69	1.0822	14.19	0.956	0.15
570	8.70	1.208	0.353	9.10	1.6693	15.08	0.953	0.15
0.01 M NaOH+0.0005 M Cl$^-$								
–320	–0.39	0.940	0.247	193.75	0.9621	13.25	0.824	0.15
–220	0.27	0.947	0.387	75.97	1.0416	11.36	0.879	0.15
–120	0.67	0.943	0.375	124.17	0.9715	10.87	0.891	0.15
–20	0.99	0.949	0.352	98.21	0.9770	11.56	0.874	0.15
70	1.16	0.948	0.327	86.95	0.9819	12.49	0.863	0.15
170	1.29	0.940	0.312	75.45	0.9265	13.80	0.860	0.15
270	1.46	0.947	0.309	53.52	0.9746	15.99	0.855	0.15
370	1.62	0.961	0.357	31.88	1.2334	17.58	0.883	0.15

***E*, mV**	***I*, μA/cm²**	**R0, kΩ·cm²**	**R1, kΩ·cm²**	**R2, kΩ·cm²**	**C1, μF/cm²**	**CPE2 Q_0, μF·cm^{-2}·s^{n-1}**	**CPE2 *n***	**Low frequency limit, Hz**
470	2.30	0.953	0.351	21.09	1.1491	17.77	0.907	0.15
570	6.95	0.963	0.308	10.11	1.4523	18.28	0.914	0.15
0.01 M NaOH + 0.001 M Cl⁻								
–380	–0.55	0.856	0.311	83.18	0.9942	14.52	0.825	0.15
–280	0.01	0.861	0.322	108.25	0.9976	12.85	0.876	0.15
–180	1.94	0.863	0.323	86.52	1.0025	12.14	0.851	0.15
–80	1.49	0.866	0.309	95.06	1.0247	11.99	0.857	0.15
70	2.00	0.861	0.281	90.35	0.9658	13.33	0.847	0.15
170	1.08	0.864	0.297	94.23	0.9943	14.07	0.860	0.15
270	1.14	0.864	0.307	67.70	1.0464	16.52	0.852	0.15
370	1.58	0.866	0.286	43.32	1.1374	19.45	0.858	0.15
470	1.80	0.868	0.281	28.56	1.1908	21.00	0.865	0.15
570	4.25	0.865	0.268	12.84	1.1956	23.42	0.859	0.15
0.01 M NaOH + 0.003 M Cl⁻								
–320	–0.74	0.807	0.333	269.25	1.0691	11.36	0.866	0.15
–220	–0.05	0.817	0.392	95.87	1.1550	10.92	0.875	0.15
–120	0.75	0.808	0.312	96.67	1.0651	11.03	0.872	0.15
–20	0.93	0.811	0.306	97.49	1.0712	11.53	0.858	0.15
70	1.00	0.815	0.254	100.45	1.2444	11.79	0.858	0.15
170	1.16	0.814	0.297	82.36	1.1120	13.21	0.856	0.15
270	1.21	0.814	0.300	62.10	1.1447	14.87	0.857	0.15
370	1.39	0.815	0.279	39.34	1.1835	17.04	0.861	0.15
470	2.36	0.816	0.268	26.29	1.1988	18.04	0.875	0.15
570	4.53	0.815	0.254	11.93	1.2444	19.36	0.880	0.15

Table 3. Calculated values of the equivalent circuit elements for 0.1 M NaOH solutions.

***E*, mV**	***I*, μA/cm²**	**R0, kΩ·cm²**	**R1, kΩ·cm²**	**R2, kΩ·cm²**	**C1, μF/cm²**	**CPE2 Q_0, μF·cm^{-2}·s^{n-1}**	**CPE2 *n***	**Low frequency limit, Hz**
0.1 M NaOH								
–340	–1.34	0.104	0.205	52.33	5.0485	10.49	0.908	0.15
–240	0.38	0.103	0.113	47.90	4.3557	11.03	0.883	0.15
–140	1.80	0.102	0.102	46.28	4.1899	12.76	0.833	0.15
–40	1.26	0.102	0.099	36.66	4.1782	11.98	0.872	0.37
70	1.42	0.103	0.102	31.39	4.4087	12.59	0.877	0.37
170	1.35	0.103	0.092	26.13	4.5079	13.64	0.883	0.20
270	2.69	0.103	0.089	16.12	4.7546	13.59	0.924	0.15
370	4.01	0.103	0.080	10.24	5.1466	15.07	0.930	0.70
470	7.84	0.103	0.072	6.12	5.4181	15.06	0.949	0.98
570	43.79	0.102	0.043	0.47	5.2948	267.46	0.820	2.6
0.1 M NaOH + 0.0005 M Cl$^-$								
–320	–1.62	0.089	0.258	82.00	5.0517	10.10	0.877	0.15
–220	–0.23	0.087	0.126	80.04	4.2635	11.96	0.856	0.15
–120	0.10	0.087	0.108	67.41	4.1133	13.19	0.830	0.15
–20	0.92	0.087	0.105	49.74	4.1821	15.26	0.805	0.15
70	0.97	0.087	0.100	32.88	4.3208	14.51	0.851	0.27
170	0.27	0.087	0.102	34.39	4.7071	14.79	0.875	0.15
270	1.40	0.087	0.101	18.05	5.1729	14.26	0.913	0.15
370	2.85	0.087	0.090	10.75	5.5358	15.96	0.910	0.70
470	4.54	0.087	0.074	6.94	6.1094	15.87	0.931	0.98
570	33.41	0.088	0.042	0.32	6.9312	330.87	0.789	3.6
0.1 M NaOH + 0.001 M Cl$^-$								
–360	–0.69	0.085	0.123	35.44	4.3031	11.22	0.904	0.15
–260	1.13	0.084	0.113	52.58	4.4795	11.36	0.865	0.15
–160	1.78	0.083	0.101	52.56	4.3658	13.24	0.819	0.15
–60	1.36	0.082	0.096	42.75	4.3173	12.73	0.858	0.27
0	1.13	0.083	0.113	41.70	4.6383	12.01	0.877	0.51

***E*, mV**	***I*, μA/cm²**	**R0, kΩ·cm²**	**R1, kΩ·cm²**	**R2, kΩ·cm²**	**C1, μF/cm²**	**CPE2 Q_0, μF·cm^{-2}·s^{n-1}**	**CPE2 *n***	**Low frequency limit, Hz**
70	1.19	0.083	0.108	35.92	4.7934	13.32	0.869	0.27
170	1.31	0.083	0.093	27.41	4.9972	14.02	0.885	0.27
270	1.63	0.083	0.087	18.38	5.3465	14.51	0.914	0.37
370	2.08	0.083	0.080	11.54	5.8045	15.34	0.931	0.51
470	2.41	0.082	0.069	7.19	6.2298	15.66	0.953	0.70
0.1 M NaOH + 0.003 M Cl⁻								
–370	–0.31	0.079	0.125	35.27	4.3654	11.87	0.897	0.15
–270	1.10	0.078	0.103	49.34	4.4057	11.20	0.878	0.15
–170	1.53	0.078	0.120	56.19	4.5799	12.61	0.833	0.15
–70	1.59	0.078	0.116	52.86	4.5806	13.82	0.820	0.15
0	1.35	0.078	0.097	48.84	4.4969	14.52	0.827	0.15
70	1.19	0.078	0.101	50.96	4.8231	15.19	0.849	0.15
170	0.09	0.078	0.094	43.84	5.2626	15.80	0.881	0.15
270	3.48	0.077	0.083	16.39	5.4155	17.65	0.879	0.15
370	3.21	0.078	0.074	11.83	5.9641	17.26	0.917	0.51
470	5.39	0.078	0.070	6.63	6.5907	16.98	0.938	0.70
570	23.68	0.078	0.036	0.36	7.3013	293.83	0.817	3.6

When analyzing the results of the fitting, it should be noted that the resistance of R0 practically does not depend on the change in potential with a constant composition of the solution. On the contrary, there is a sharp decrease in the resistance R0 as the total concentration of ions in the solution increases, affecting the conductivity of the electrolyte. Previously, we showed the presence of a linear correlation between the tabular and measured conductivities of alkali solutions without additives [26]. Currently, such a calculation has not been carried out for solutions with chloride additives, however, it is obvious that the specific electrical conductivity of the solution is inversely proportional to the resistance R0 and increases with an increase in the total concentration of ions in the electrolyte. The strongest effect on R0 is exerted by the addition of chloride to the solution with the lowest concentration of alkali, since its conductivity itself is minimal. Thus, the same addition of 0.03 M Cl^- to an electrolyte with 0.001 M NaOH reduces the resistance of R0 by 75%, and in more well-conducting solutions of 0.01 M NaOH and 0.1 M NaOH by 29% and 24%, respectively. In any case, the resistance R0 is not related to the state of the nickel surface.

Figure 4 shows the dependence of the resistance R1, due to charge transfer through the oxide layer on the nickel surface, on the potential of the electrode at different concentrations of the solution components. Obviously, this parameter of the model is almost independent of polarization. Only in the most concentrated solutions (0.1 M NaOH) there is a noticeable decrease in the resistance of R1 in the potential range above +370 mV, where the formation of pitting corrosion begins and thermodynamic oxygen release is possible. On the contrary, it can be seen that the values of R1 form a plateau of values, ranked depending on the total concentration of ions in the solution. With a minimum alkali content (0.001 M NaOH), comparable concentrations of chloride additives significantly affect the total ion concentration (and electrolyte conductivity), which has a noticeable effect on R1. With an increase in the concentration of alkali by one and two orders of magnitude, the effect of small chloride additives becomes less significant and less affects the value of R1.

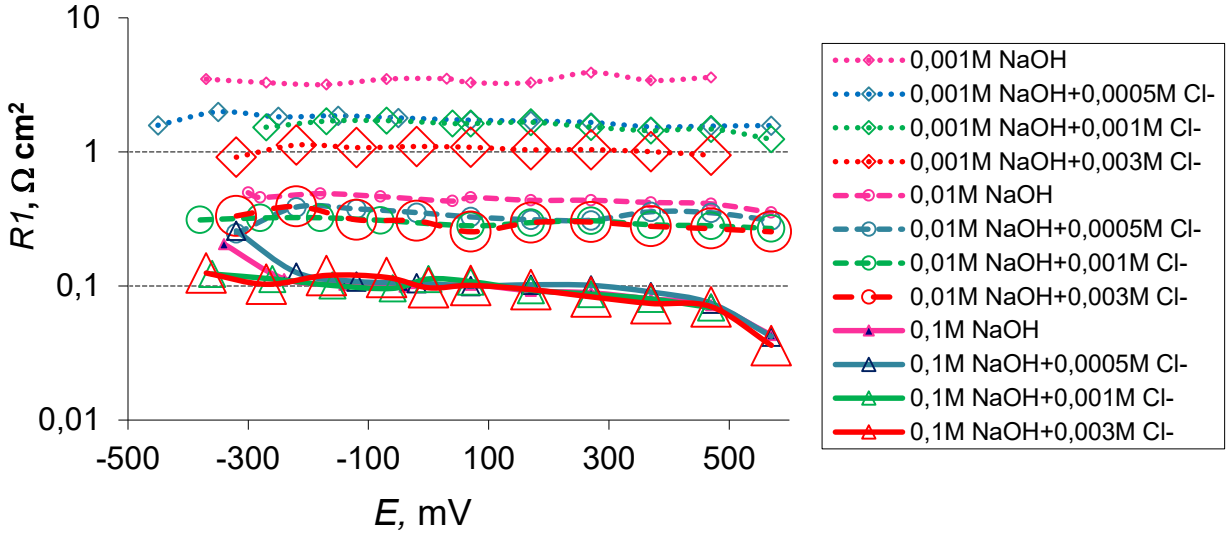

Figure 4. Dependence of the charge transfer resistance through the oxide layer R1 on the potential for alkaline solutions with different chloride content

If we average the values of R1 in the potential range, where this parameter changes little (from –300 mV to +300 mV), and build a dependence on the logarithm of the total concentration of ions in solution (Figure 5), these data are described by an equation of the exponential type:

$$\mathrm{R1} = k \cdot C^{-m}, \qquad (2)$$

where k is a constant, C is the concentration of ions in solution and m is the exponent.

For this system, the parameters of this equation turned out to be: $k = 0.0174$ and $m = 0.714$ with a correlation coefficient $R^2 = 0.970$, indicating adequate compliance with experimental results.

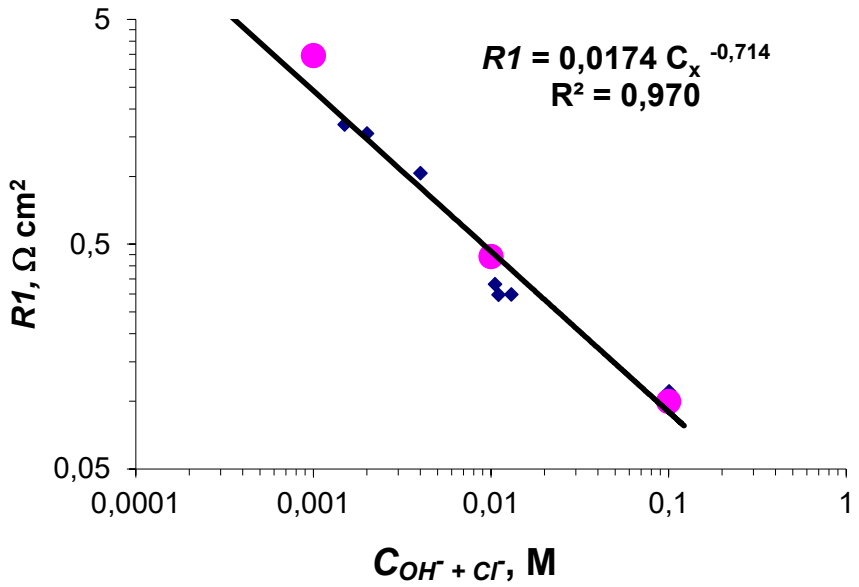

Figure 5. Dependence of the charge transfer resistance R1 of the barrier oxide–hydroxide layer on the total concentration of anions in solution. Large purple dots indicate solutions that do not contain chlorides.

Previously we studied of a similar system in alkali solutions without additives. It has been shown [26] that such a dependence of resistance on the alkali concentration corresponds to a model in which the current at the oxide film–solution interface is due to activated charge transfer of OH^- anions through the electric double layer C1. For ion penetration from the state of the adsorption plate into the surface film it must be overcome by the activation barrier, the height of which will be affected by the electric field strength. Then formally, the charge transfer current through the barrier can be expressed as:

$$I_{ct} = I_0 \cdot C_a \exp(-A/R \cdot T + n \cdot F \cdot \xi / R \cdot T), \quad (3)$$

where C_a is the ions concentration in the adsorption plate, A is the activation energy, n is the charge, R and F are the universal gas constant and the Faraday number, ξ is the potential drop in the double layer (more precisely, between the outer plate and the activated complex), I_0 is the current at a single concentration and zero value under the exponent (when the electric field eliminates the activation barrier).

Differentiating equation (3) by potential, we obtain the conductivity of the system σ:

$$\sigma = dL/dE = I_0 \cdot C_a \cdot n \cdot F / R \cdot T \exp(-A/R \cdot T + n \cdot F \cdot \xi) / R \cdot T). \quad (4)$$

Since the resistance R is inversely proportional to the conductivity:

$$R = (I_0 \cdot C_a \cdot n \cdot F / R \cdot T)^{-1} \exp(A/R \cdot T - n \cdot F \cdot \xi / R \cdot T). \quad (5)$$

It is known that the concentration of ions C_a in the adsorption plate is related to the volume concentration C with the Freundlich isotherm:

$$C_a = K \cdot C^m, \quad (6)$$

where K is a constant, m is an exponent lying in the range from 0.1 to 1.

By combining (5) and (6) equations, it is possible to obtain a dependence of resistance on the concentration of ions in solution corresponding to the experimentally obtained Equation 2.

In this study, we used alkaline solutions with chloride additives. Therefore, a good description of the experimental data by Equation 1, in which C represents the total concentration of hydroxyl and chloride, indicates that both types of ions participate in the activated charge transfer. Thus, it is the patterns of activated charge transfer in the EDL field, and not the ohmic resistance of the surface film, that have a decisive influence on the resistance of R1. The resistance of the latter, of course, should change during the oxidation of nickel (during anodic polarization over time), but it is obviously much lower than the resistance of activated charge transfer and its contribution is minimal.

The dependence of the overall capacitance of the EDS on the surface of oxidized nickel on the total concentration of ions in the electrolyte and the polarization potential is shown in Figure 6. The capacitance C1 increases progressively with an increase in the concentration of components in the solution and depends slightly on the potential of the electrode in the studied boundaries. Only in the most concentrated alkaline solutions, there is a slight increase in C1 in the region of high potentials.

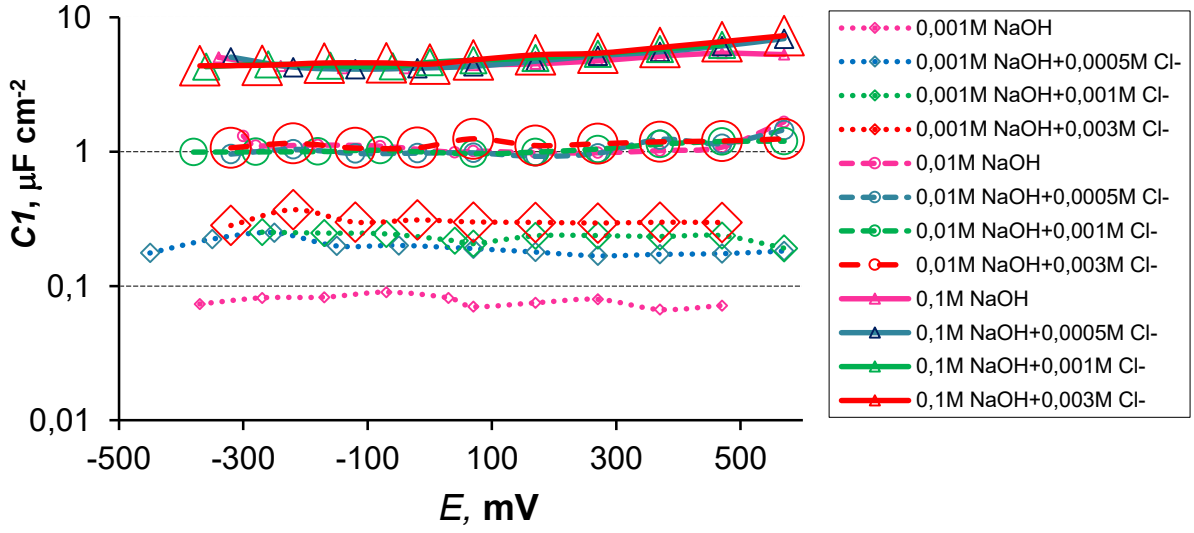

Figure 6. Dependence of the EDL capacitance on the potential for alkaline solutions with different chloride content.

The dependence of the electrical double layer capacitance C1 on the square root of the total concentration of ions in solution is based on the averaged values of the capacitance (see Figure 7).

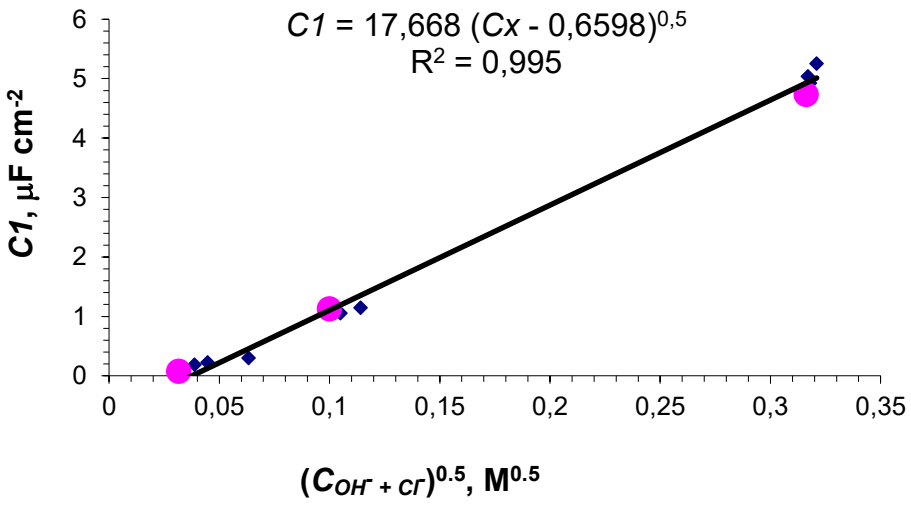

Figure 7. Dependence of the EDL capacitance on the root of the total concentration of anions in solution. Large purple dots indicate solutions that do not contain chlorides.

A linear dependence with a correlation coefficient R^2=0.995 is obtained, therefore, this process obeys the Gui–Chapman theory for specific ion adsorption on the electrode surface. Although the addition of chloride ions to the solution (blue dots) has practically no effect on the course of the approximating straight line, which tends more towards the values for alkali solutions without additives (large purple dots), a certain trend can still be noticed. In the most concentrated 0.1 M NaOH solution, the addition of chlorides still provides a slight increase in capacitance compared to the approximating line, which may indicate an increase in the specific absorption of these ions relative to hydroxyl ions.

Thus, the capacitance of C1 element depends mainly on the concentration of ions in solution and turned out to be insensitive to changes in the thickness of the oxide–hydroxide film on the nickel surface formed during anodic polarization while the impedance spectrum was taken.[3] In general, the discovered patterns of the predominant dependence of the elements R1 and C1 on the concentration of ions in solution explain the constancy of the high-frequency arcs radii in the of the hodographs with a change in polarization.

Low-frequency processes in Mansfeld's model are represented by elements R2/CPE2 of a parallel circuit responsible for the parameters of the electrochemical processes on metal Ni under an oxide layer. In this paper, we did not set out to investigate the kinetics of nickel oxidation during anodic polarization. The works of other authors are devoted to this [28, 29]. It is for elements simulating a low-frequency process that the predominant effect of the polarization potential is observed compared to the ion concentrations in the electrolyte. Graphs of the dependences for R2 resistance of the Faraday nickel oxidation process and the corresponding pseudo-capacitance represented by the CPE2 element are shown in

[3]Recording each impedance spectrum took 30–40 minutes.

Figures 8.1–8.3. Their fundamental difference from the behavior of the elements of the above-described R1/C1 scheme is obvious. It is for these elements that the predominant effect of the polarization potential is observed in comparison with the concentration of ions in the electrolyte.

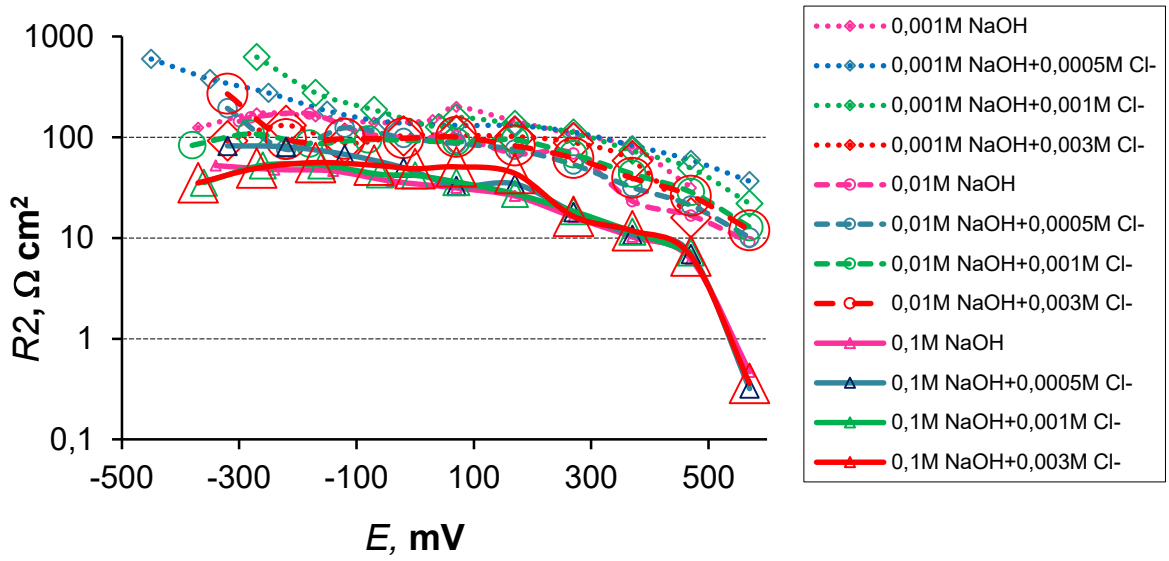

Figure 8.1. Dependence of the resistance R2 of the Faraday solid-phase oxidation of nickel on the potential for alkaline solutions with different chloride contents.

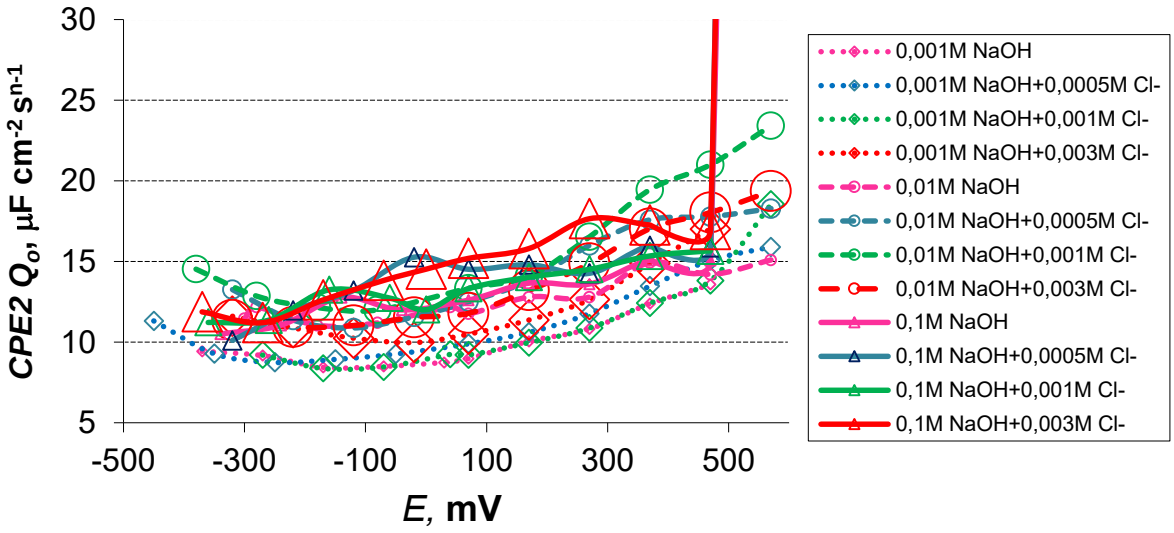

Figure 8.2. Dependence of the capacitance the Faraday oxidation process on Ni electrode, calculated from the model (Q_0 module of CPE2 element) on the potential for alkaline solutions with different chloride contents.

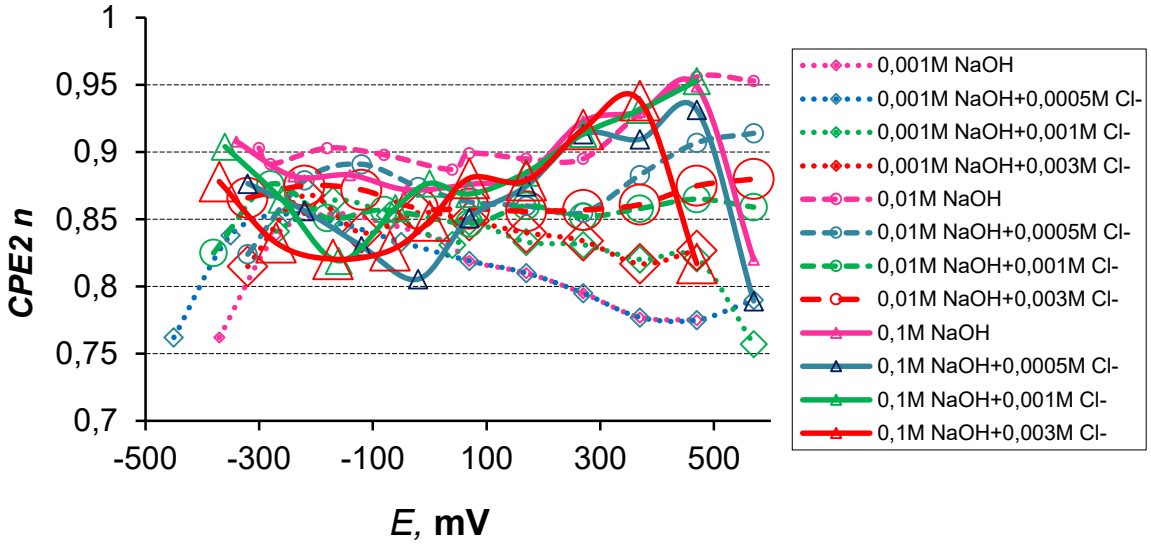

Figure 8.3. Dependence of the phase factor of CPE2 *n* on the potential for alkaline solutions with different chloride contents.

Figure 8.1 shows that the resistance R2 naturally decreases with increasing anode polarization, since the solid-state oxidation of nickel increases. The logarithmic scale of the resistance axis of the graph highlights the intensity of this influence. This is especially pronounced in the most concentrated decimole solution of sodium hydroxide, and chloride additives further enhance this effect. It is well known that nickel oxidation increases with increasing alkali concentration, especially in the presence of chlorides. In addition, the latter reduce the potential of pitting formation [15, 17–23]. In our experiments, we consistently increased the anode potential by 100 mV, so the exact value of the potential for pitting is unknown. However, their occurrence at a certain potential can be determined from Tables 1–3 by increasing the specified low-frequency boundary for processing the results in order to exclude the pseudo-inductive loop in the impedance spectra. It is obvious that with an increase in the chloride content, especially in more concentrated alkaline solutions, the potential above which pseudo-inductive loops begin to appear in the low-frequency region of the impedance spectra decreases.

The capacitive characteristics of the process of solid-phase nickel oxidation can be assessed by the modulus Q_0 of the constant-phase element CPE2.Since the phase coefficient *n* ranges from 0.75 to 0.95 (Figure 8.3), this element has a capacitive nature with a diffuse structure of the capacitor plates and/or heterogeneity of their physical-chemical properties. As the phase factor *n* is about 1, the Faraday capacitance in $\mu F \cdot cm^{-2}$ will be numerically close to the modulus Q_0 of the CPE2 element in $\mu F \cdot cm^{-2} \cdot s^{n-1}$.

Unlike element C1, due to the capacitance of the EDL, which occurs, as with any type of electrode[4], element CPE2 is by nature Faraday's pseudo-capacitance that occurs only when an oxidation-reduction process occurs on the surface. The products of these

[4]It is observed for both perfectly and imperfectly polarized electrodes.

electrochemical reactions, adsorbed on the surface, create a certain charge, the value of which depends on the filling degree and varies depending on the electrode. Therefore, Faraday's pseudo-capacitance strongly depends on the electrode potential and the nature of the reaction [30]. From Figure 8.2 it evident that Faraday's capacitance increases with increasing anode polarization and, in general, increases slightly with increasing concentrations of alkali and chloride. On average, the capacitance values range from $\mu F \cdot cm^{-2}$, which is common for many electrochemical systems. Only for highly concentrated alkali solution without and with chloride additives at the highest anode potentials +470 and +570 mV abnormally high values were obtained, probably caused by a strong distortion of the impedance hodograph shape and an increase in the error during the formal use of this equivalent scheme, even with narrowing of the frequency boundaries.

Conclusions

1. Systematic studies of the frequency spectra of the impedance on nickel in alkaline solutions in the concentration range from 0.001 M to 0.1M NaOH with chloride ion content from 0 to 0.003 M have shown that two characteristic semicircles in the Nyquist diagram are associated with processes implemented at the solution–oxide film interfaces and the oxide film–metal interface.
2. At high anodic potentials, pseudo-inductive loops may appear on the Nyquist diagram in the low frequency region due to the appearance of pitting corrosion. However, if we exclude low-frequency sections of the spectra when these loops appear, all impedance spectra can be adequately described in terms of Mansfeld's equivalent circuit.
3. The regularities of the high-frequency section of the impedance spectra are due to the properties of the R1/C1 elements, which connected in parallel. Both of these elements practically do not change with increasing electrode potential and depend mainly on the total ions concentration in the solution.
4. The nature of the concentration dependence for the elements R1 and C1 allows us to associate these elements with the regularities of the formation of an electric double layer on the electrode and activated charge transfer by OH^- and Cl^- ions in the field of EDL.
5. The low-frequency section of the impedance spectrum described by the R2/CPE2 elements is due to Faraday's processes of nickel oxidation, which strongly depend on the potential and concentration of the electrolyte.
6. For the system under study, it turned out that, based on the values of the surface resistance R1 and the overall capacitance C1 of EDL, it is impossible to track the change in the thickness of the oxide layer formed on the surface during anodic polarization. Probably, the contribution of the ohmic resistance of this layer is small compared to the resistance of the activated charge transfer in the EDL field, and the contribution of changes in the thickness and dielectric properties of the layer is insufficient to affect the value of R1 and C1.

References

1. I.K. Garkushin, O.V. Lavrentieva, M.A. Istomova and N.Yu. Kalmykov, *Structural materials: composition, properties, application*, Samara State Technical University, 2015, p. 238 (in Russian).
2. A.A. Bagerman and A.Z. Zhivushkin, The opportunity to address the issues on the structural fatigue strength of turbine blades using the prediction of the high-temperature endurance limit of the material of heat-resistant nickel-based alloys, *Tyazheloye Mashinostroyeniye*, 2022, no. 1–2, 7–9 (in Russian).
3. B.A. Kalin, Non-ferrous metals in material physics of National Research Nuclear University MEPhI, *Non-ferrous metals*, 2014, **12**, 11 (in Russian).
4. A.G. Oschepkov and E.R. Savinova, Nickel catalysts for the electro oxidation of hydrogen and borohydride: Current state and prospects, *Kinet. Catal*., 2022, **63**, no. 1, 16–32 (in Russian). doi: 10.31857/s0453881122010130
5. D.S. Hall, D.J. Lockwood, C. Bock and B.R. MacDougall, Nickel hydroxides and related materials: a review of their structures, synthesis and properties, *Proc. R. Soc. A*, 2015, **471**, no. 2, 1–65. doi: 10.1098/rspa.2014.0792
6. E.B. Ferreira and G. Jerkiewicz, On the electrochemical reduction of β-$Ni(OH)_2$ to metallic nickel, *Electrocatalysis*, 2021, **12**, 199–209. doi: 10.1007/s12678-021-00643-0
7. E.B. Ferreira, S. Tahmasebi and G. Jerkiewicz1, On the catalytic activity and corrosion behavior of polycrystalline nickel in alkaline media in the presence of neutral and reactive, *Electrocatalysis*, 2021, **12**, 146–164. doi: 10.1007/s12678-020-00637-4
8. N.I. Ostanin, V.M. Rudoy, T.N. Ostanina and A.B. Darintseva, *Theory and technology of obtaining non-ferrous metals by electrolysis*, Ural Federal University, Yekaterinburg, 2022, 174 (in Russian).
9. I.D. Kudryavtseva, V.I. Balakai, G.P. Smetankin and K.V. Balakai, Regularities of nickel electrodeposition from a low-concentration chloride electrolyte for anticorrosive coatings, *Bulletin of the all-Russian scientific research and design institute of electric locomotive engineering*, 2007, no. 1, 98–107 (in Russian).
10. E. Gbmez, R. Pollina and E. Vall, Morphology and structure of nickel nuclei as a function of the conditions of electrodeposition, *J. Electroanal. Chem*., 1995, **397**, 111–118. doi: 10.1016/0022-0728(95)04202-1
11. V. Makarova, D.S. Kharitonov, I.B. Dobryden and A.A. Chernik, Corrosion behavior in acid and alkaline media of nickel coatings deposited at room temperature, *Russ. J. Appl. Chem*., 2018, **91**, no. 9, 1441−1450. doi: 10.1134/S1070427218090069
12. M.V. Lukyanenko, Energy model of nickel-hydrogen batteries, *The Siberian Aerospace Journal*, 2005, **4**, no. 7, 67–71 (in Russian).
13. A.A. Savina, A.O. Boev, E.D. Orlova, A.V. Morozov and A.M. Abakumov, Nickel is a key element of the energy of the future, *Russian Chemical Reviews*, 2023, **92**, no. 7, RCR5086 (in Russian). doi: 10.59761/RCR5086

14. V.V. Parshutin, N.L. Bogdashkina and G.P. Chernova, The influence of the medium on the corrosion and electrochemical behavior of nickel, *Prot. Met.*, 2007, **43**, no. 1, 64–70. doi: 10.1134/S0033173207010080
15. A.B. Kilimnik and E.Y. Nikiforova, Electrochemical behavior of nickel and its oxides in concentrated solutions of sodium hydroxide, *Russ. J. Electrochem.*, 2013, **49**, 1122–1126. doi: 10.1134/S1023193513120033
16. S.S. Fomanyuk, Y.S. Krasnov and G.Y. Kolbasov, Kinetics of electrochromic process in thin films of cathodically deposited nickel hydroxide, *J. Solid State Electrochem.*, 2013, **17**, 2643–2649. doi: 10.1007/s10008-013-2169-1
17. N. Sridhar and D.S. Dunn, *In Situ* Study of Salt Film Stability in Simulated Pits of Nickel by Raman and Electrochemical Impedance Spectroscopies, *J. Electrochem. Soc.*, 1997, **144**, no. 12, 4243–4253. doi: 10.1149/1.1838173
18. E.Yu. Nikiforova and A.B. Kilimnik, Electrochemical behavior of air-oxidized nickel in concentrated solutions of sodium hydroxide, *Bulletin of the Tambov State Technical University*, 2009, **15**, no. 1, 147–152 (in Russian).
19. Z.I. Kudryavtseva, L.A. Burkal'tseva and A.G. Pshenichnikov, Surface properties of nickel electrodes in an alkaline electrolyte: an ellipsometry study, *Russ. J. Electrochem.*, 2004, **40**, no. 11, 1208–1213. doi: 10.1023/B:RUEL.0000048656.31084.12
20. A.I. Shcherbakov, L.P. Kornienko, I.V. Kasatkina, I.G. Korosteleva and V.N. Dorofeeva, Pitting corrosion of nickel in a slightly alkaline NaOH solution in the presence of chloride ions. In the collection: Physico-chemical processes in condensed media and at interphase boundaries (PHAGRAN-2018), *VIII All-Russian conference with international participation dedicated to the 100th anniversary of Voronezh State University*, Voronez, Voronez State University, 2018, 213–214 (in Russian).
21. I.I. Zamaletdinov, Pitting on passive metals, *Prot. Met.*, 2007, **43**, 470–475. doi: 10.1134/S0033173207050098
22. F. Mansfeld, M.W. Kending and S. Tsai, Recording and analysis of ac impedance data for corrosion studies, *Corrosion*, 1981, **37**, no. 5, 301–307. doi: 10.5006/1.3621688
23. L.P. Kornienko, V.E. Kasatkin, A.I. Scherbakov, I.G. Korosteleva, I.V. Kasatkina and V.N. Dorofeeva, Electrochemical studies of the state of a nickel surface in an alkaline medium, *Prot. Met. Phys. Chem. Surf.*, 2022, **58**, 1213–1219. doi: 10.1134/S2070205122070061
24. Z. Szklarska-Smialowska and R. Krishnakumar, Ellipsometry in studies of metallic corrosion and oxidation, *Electrochemical and Optical Techniques for the Study and Monitoring of Metallic Corrosion*, NATO ASI Series, Springer, Dordrecht., 1991, **203,** 285–354. doi: 10.1007/978-94-011-3636-5-9
25. P. Marcus and J.M.H. Herbelin, The entry of chloride ions into passive films on nickel studied by spectroscopic (ESCA) and nuclear (^{36}Cl radiotracer) methods, *Corros. Sci.*, 1993, **34**, no. 7, 1123–1145. doi: 10.1016/0010-938X(93)90293-P

26. V.E. Kasatkin, L.P. Kornienko, A.I. Shcherbakov, I.G. Korosteleva, I.V. Kasatkina and V.N. Dorofeeva, Effect of sodium hydroxide concentration on nickel surface state: experience in EIS methods applying, *Electrocatalysis*, 2022, **13**, 539–550. doi: 10.1007/s12678-022-00735-5
27. A.M.R. Reynoso, J.C.T. González, C.O.G. Morán, J.G.M. Hernández, A.M. Ruiz, J.M. Hernández and R.O. Cruz, Electrochemical impedance spectroscopy (EIS): A Review study of basic aspects of the corrosion mechanism applied to steels, *Electrochemical Impedance Spectroscopy First Editon*, IntechOpen, 2020. doi: 10.5772/intechopen.94470
28. V.S. Bagotzky, N.A. Shumilova, G.P. Samoilov and E.I. Khrushcheva, Electrochemical oxygen reduction on nickel electrodes in alkaline solutions, *Electrochim. Acta*, 1972, **17**, no. 9, 1625–1635. doi: 10.1016/0013-4686(72)85053-9
29. E.B. Ferreira, S. Tahmasebi and G. Jerkiewicz, On the catalytic activity and corrosion behavior of polycrystalline nickel in alkaline media in the presence of neutral and reactive gases, *Electrocatalysis*, 2021, **12**, 146–164. doi: 10.1007/s12678-020-00637-4
30. Modern aspects of electrochemistry, Edited by J. Bokris and B.E. Conway, Mir, Moscow, 1967, 509 (in Russan).
31. H. Bode, K. Dehmelt and J. Witte, Zur kenntnis der Nickelhydroxidelektrode–I. Uber das nickel (II)-hydroxidhydrat, *Electrochim. Acta*, 1966, **11**, no. 8, 1079–1087. doi: 10.1016/0013-4686(66)80045-2
32. N. Sato, The stability of localized corrosion, *Corros. Sci*, 1995, **37**, no. 12, 1947–1967. doi: 10.1016/0010-938X%2877%2990002-6
33. Yu.I. Kuznetsov and O.A. Lukyanchikov, Initiation and inhibition of pitting on nickel in neutral solutions, *Prot. Met*., 1988, **24**, no. 2, 182–188 (in Russian).
34. D.S. Hall, C. Bock and B.R. MacDougall, The electrochemistry of metallic nickel: oxides, hydroxides, hydrides and alkaline hydrogen evolution, *J. Electrochem. Soc*., 2013, **160**, no. 3, F235–F243. doi: 10.1149/2.026303jes

♦ ♦ ♦